Original Article

Thermally integrated microchannel methanol steam reforming reactors for hydrogen production

Junjie Chen

Department of Energy and Power Engineering, School of Mechanical and Power Engineering, Henan Polytechnic University, 2000 Century Avenue, Jiaozuo, Henan, 454000, P.R. China

ARTICLE INFO

ABSTRACT

Thermally integrated microchannel reforming reactors have attracted considerable interest for a wide variety of applications. However, the mechanisms for the effects of design factors on heat transfer characteristics are still not fully understood. The present study relates to a thermochemical process for producing hydrogen by the catalytic endothermic reaction of methanol with steam in a thermally integrated microchannel reforming reactor. Numerical simulations are conducted using computational fluid dynamics to understand the consumption, generation, and exchange of thermal energy between endothermic and exothermic processes in the reactor. The effects of wall heat conduction properties and channel dimensions on heat transfer characteristics and reactor performance are investigated. Thermodynamic analysis is performed based on specific enthalpy to better understand the evolution of thermal energy in the reactor. The results indicate that the thermal conductivity of the channel walls is fundamentally important. Materials with high thermal conductivity are preferred for the channel walls. Thermally conductive ceramics and metals are well-suited. Wall materials with poor heat conduction properties degrade the reactor performance. Reaction heat flux profiles are considerably affected by channel dimensions. The peak reaction heat flux increases with the channel dimensions while maintaining the flow rates. The change in specific enthalpy is positive for the exothermic reaction and negative for the endothermic reaction. The change in specific sensible enthalpy is always positive. Design recommendations are made to improve thermal performance for the reactor.

1. Introduction

The steam reforming of hydrocarbon or alcohol fuels has attracted increasing interest in the context of the production of hydrogen [1, 2]. Typically, a traditional steam reforming reactor system consist of a reformer, which contains an appropriate reforming catalyst to facilitate the endothermic reforming reaction and a large industrial furnace to provide the necessary thermal energy for the reaction [3, 4]. A hydrocarbon or alcohol fuel and steam are supplied to the reformer, and hydrogen must be separated from the undesired product, carbon monoxide. An industrial steam methane reforming reactor typically contains an array of long and narrow tubes [5, 6], which are usually made of refractory alloys. The interiors of the tubes constitute the reaction region and the tubes are packed with commercial porous pellets of material, which

are impregnated with an appropriate reforming catalyst. The heated length of the tubes is typically between 6 and 12 meters and the diameter of the tubes varies between 9 and 16 cm. The tubes are situated within the combustion chamber of the furnace. With respect to steam methane reforming processes, flame temperatures as high as 1300 °C are typically employed to ensure that the temperature of the reaction lies within a range of about 800 to 900 °C [7, 8]. The furnace operates at temperatures considerably higher than the temperatures required by the reaction. High flame temperatures up to about 1300 °C are required in order to ensure that the reforming catalyst operates at the desired temperatures. However, high flame temperatures will inevitably cause the formation of nitrogen oxide. Furnace designs vary, but the volume is necessarily large.

Unfortunately, such industrial steam reforming reactors cannot be scaled to smaller dimensions for a modular portable unit so as to provide a sufficient hydrogen-rich reformed gas for a chemical reaction process or a fuel cell. For example, portable fuel cell systems can be used for power generation [9, 10]. Portable fuel cell systems are of particular interest in remote or inaccessible areas [11, 12] and in undeveloped countries, which lack technological capability, a power grid, and the funds for an extensive electricity distribution infrastructure. Fuel cell vehicles are another area of interest, particularly for mass transit vehicles and trucks and for hybrid vehicle power trains [13, 14]. High purity hydrogen in high-pressure tanks is presently not desirable for fuel cell vehicles due to the volume and safety constraints. Consequently, the optimum solution will be the use of liquid hydrocarbon fuels, such as heptane [15, 16] and liquefied natural gas [17, 18], or the use of volatile fuels, such as alcohols [19, 20] and motor grade kerosene [21] and gasoline [22], in order to feed an on-board reforming reactor and produce form a hydrogen-rich product gas, commonly referred to as reformate, as the feedstock for fuel cell vehicles.

To solve the problems outlined above, various plate-type reforming reactors have been developed. These reactors are compact in size. Even at low temperatures, catalytic combustion can be carried out in such reactors. An example of such plate-type reforming reactors has been developed by Koga et al. [23]. The reforming reactor has alternating flat gap spaces for a fuel-air mixture and a fuel-steam mixture. The reforming gap spaces are filled with a reforming catalyst, while the combustion gap spaces are filled with a combustion catalyst. The temperatures are substantially lower than 1300 °C. A more compact example of the plate-type reforming reactor has been developed by Igarashi et al. [24]. A rectangular wall reactor has been designed, which consists of alternating stages comprising a heated reformer area separated from a conductive heating area [25, 26]. Each stage comprises a plurality of plates. For example, each stage is formed from three plates, a center partition plate and a pair of spaced boundary plates. A catalyst is deposited by applying electroless plating on the plate surfaces of the reforming reactor. The compact reforming reactor can achieve higher conversions than traditional reactors due to increased surface area for heat transfer.

However, the above plate-type reforming reactors have not been widely used, and the difficulties of design are a primary concern. For the plate-type reforming reactor described above [23], the reforming and combustion catalysts used to fill the gaps between the channel plates are in the form of pellets or particles. The catalyst systems do not adhere to the channel walls. As a result, the heat released by the exothermic catalytic combustion reaction must be transferred to the gas phase before reaching the reforming catalyst. Thermal energy is therefore transferred

ineffectively within such a reaction system. Additionally, the reaction volume of the reactors is usually large, since a gaseous stream transfers the heat of reaction. For the compact plate-type reforming reactor described above [24], the reforming catalyst is deposited onto the walls of the reforming channels. Consequently, the heat of reaction must be transferred via thermal conduction to the reforming catalyst through the thermally conductive walls of the reactor, and in the combustion channels heat transfer still takes place between the fluid phase and the solid phase.

Another thermally integrated tubular-type reforming reactor has been developed by Ioannides and Verykios [27]. The tubular reactor consists of an inner non-porous ceramic channel with a high thermal conductivity and an outer U-shaped ceramic channel, with a structure of an endocentric construction. Additionally, the inside and outside surfaces of the inner channel are coated with similar or different metal catalyst layers [27, 28]. A reactant mixture consisting of methane and oxygen is introduced into the inner channel. The reaction mixture passes into the inner channel, thereby carrying out a combustion reaction by utilizing a catalyst. The reaction mixture then passes out the inner channel and passes into an annulus space between the inner and outer channels in the reverse direction. In the annulus space, a reforming reaction takes place within the reforming catalyst layer. The design makes the reforming reactor more compact. However, the design is usually employed on a laboratory scale.

Accordingly, further study is needed to take the inherent myriad advantages associated with the tubular reactor. Design methods must also be developed to address the issues associated with scale-up of such continuous flow reactors. Recently, a thermally integrated microchannel chemical reactor has been developed for simultaneously conducting exothermic and endothermic reactions [29, 30]. The reactor consists of two separate sets of flow channels in an alternating, layered arrangement [31, 32]. The reactor comprises an exothermic heat exchange layer and an endothermic process layer [33, 34]. The dividing walls of the reactor have the same or different catalysts on opposed surfaces, which are selected for a particular reaction occurring in the adjacent reaction region [35, 36]. A microchannel reforming reaction system can be formed by stacking modular reactor units [37, 38] to achieve any desired throughput capacity and portability [39, 40]. Methods have also been suggested for the catalytic reforming of hydrocarbon fuels for the production of hydrogen or synthesis gas by utilizing such a reactor [41, 42]. There is a continuing effort to perform steam reforming reactions in microchannel chemical reactors [43, 44]. However, the mechanisms for the effects of design factors on heat transfer characteristics are still not fully understood.

This study relates to a thermochemical process for producing hydrogen by the catalytic endothermic reaction of methanol with steam in a thermally integrated microchannel reforming reactor. Computational fluid dynamics simulations are conducted to better understand the consumption, generation, and exchange of thermal energy in the reactor. The effects of wall heat conduction properties and channel dimensions on heat transport characteristics and reactor performance are investigated. The objective of this study is to gain insight into the fundamental characteristics of heat transfer in thermally integrated microchannel reforming reaction systems. Particular emphasis is placed on the dependence of heat transfer characteristics on wall heat conduction properties and channel dimensions in various situations, with an attempt to improve the distribution of thermal energy for use in microchannel reforming reaction systems.

2. Description of the Model
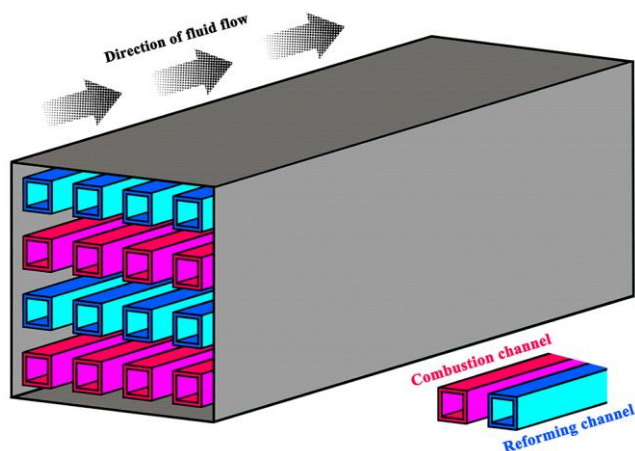
2.1. Description of the reactor

Fig. 1. Schematic illustration of the microchannel methanol reforming reactor used for hydrogen production. The catalyst layers are illustrated but the channel walls are not depicted for clarity.

The present study relates to a thermally integrated microchannel methanol reforming reactor. The reactor consists of a set of combustion channels and a set of reforming channels in an alternating arrangement. The thermally integrated microchannel reactor is depicted schematically in Fig. 1. The straight channels can be configured and manifolded for simultaneous passage of different process reactant streams with flow paths in counter-current, cross-flow, or co-current flow modes [45, 46]. Each channel contains a layer of catalyst, as depicted schematically in Fig. 1. A reactant stream of methanol and air is introduced into the combustion channels and a reactant stream of methanol and steam is introduced into the reforming channels. The flow paths are configured in the reactor to thermally contact exothermic and

endothermic reactant streams in adjacent channels. A high temperature exothermic reaction takes place in the combustion channels. No flame combustion is involved in the process. The catalyst layers in each channel are designed in an opposed relationship. In this arrangement, the heat transfer within the reactor will be highly efficient [45, 46]. The catalytically active surface area or catalyst loading can be balanced for the reactor [47, 48], thereby avoiding heat imbalances within the reactor or reducing the likelihood of the formation of hot spots.

The temperature of the reactant streams is 373 K at the flow inlets with a pressure of 2.0 MPa, since optimum reactor operating conditions lie at medium pressures of 2.0-3.0 MPa [49]. The equivalence ratio of fuel to air is 0.8, since lean mixtures are more efficient. The steam-to-carbon molar ratio is 1.4. Excess of steam is required to reduce the amount of carbon monoxide produced and avoid coke formation [50]. The velocity of the process reactant stream and the combustible reactant stream is 2.0 and 0.6 m/s, respectively, at the flow inlets. The overall thermal balance within the reactor can be achieved within a range of the reforming-to-combustion velocity ratio from 3.0 to 3.5 [51]. The channels are illustrated in Fig. 1 by way of example, and channels of any shape and dimension may be used. In the present study, the cross-sectional shape of the channels is square, with a side length of 0.7 mm. The channels are 50.0 mm in length, since the reactor must be of sufficient length to allow the reforming reaction to proceed to the required conversion. The catalyst layers and the channel walls are 0.1 and 0.7 mm, respectively, in thickness. The thickness of the catalyst layers is taken as an independent parameter in order to understand how important thermal management is. The channel walls must be of sufficient thickness and strength to maintain the integrity of the channels [52]. At room temperature, the thermal conductivity, which indicates the ability to conduct heat, of the channel walls is 200 W/(m·K). The design with high wall thermal conductivity will lead to improved heat transfer and therefore chemical conversion.

2.2. Mathematical model

The model consists of channel walls with the adjacent combustion and reforming half-channels in a co-current flow configuration. The mathematical model is solved and implemented in ANSYS FLUENT to obtain the problem solution. ANSYS FLUENT permits multi-dimensional modeling of physical and chemical phenomena in the processes.

The continuity equation is given by

$$\frac{\partial(\rho u_x)}{\partial x} + \frac{\partial(\rho u_y)}{\partial y} + \frac{\partial(\rho u_z)}{\partial z} = 0, \qquad (1)$$

where x, y, and z are coordinate variables, ρ is the density, and u is the velocity.

The momentum conservation equations can be written as

$$-\frac{\partial p}{\partial x} - \frac{\partial}{\partial x}\left[\frac{2}{3}\mu\left(\frac{\partial u_{xx}}{\partial x} + \frac{\partial u_{yx}}{\partial y} + \frac{\partial u_{zx}}{\partial z}\right)\right] + \frac{\partial}{\partial x}\left[\mu\left(\frac{\partial u_x}{\partial x} + \frac{\partial u_x}{\partial x}\right)\right]$$
$$+\frac{\partial}{\partial y}\left[\mu\left(\frac{\partial u_x}{\partial y} + \frac{\partial u_y}{\partial x}\right)\right] + \frac{\partial}{\partial z}\left[\mu\left(\frac{\partial u_x}{\partial z} + \frac{\partial u_z}{\partial x}\right)\right] = 0 \quad , \quad (2)$$

$$-\frac{\partial p}{\partial y} - \frac{\partial}{\partial y}\left[\frac{2}{3}\mu\left(\frac{\partial u_{xy}}{\partial x} + \frac{\partial u_{yy}}{\partial y} + \frac{\partial u_{zy}}{\partial z}\right)\right] + \frac{\partial}{\partial x}\left[\mu\left(\frac{\partial u_y}{\partial x} + \frac{\partial u_x}{\partial y}\right)\right]$$
$$+\frac{\partial}{\partial y}\left[\mu\left(\frac{\partial u_y}{\partial y} + \frac{\partial u_y}{\partial y}\right)\right] + \frac{\partial}{\partial z}\left[\mu\left(\frac{\partial u_y}{\partial z} + \frac{\partial u_z}{\partial y}\right)\right] = 0 \quad , \quad (3)$$

$$-\frac{\partial p}{\partial z} - \frac{\partial}{\partial z}\left[\frac{2}{3}\mu\left(\frac{\partial u_{xz}}{\partial x} + \frac{\partial u_{yz}}{\partial y} + \frac{\partial u_{zz}}{\partial z}\right)\right] + \frac{\partial}{\partial x}\left[\mu\left(\frac{\partial u_z}{\partial x} + \frac{\partial u_x}{\partial z}\right)\right]$$
$$+\frac{\partial}{\partial y}\left[\mu\left(\frac{\partial u_z}{\partial y} + \frac{\partial u_y}{\partial z}\right)\right] + \frac{\partial}{\partial z}\left[\mu\left(\frac{\partial u_z}{\partial z} + \frac{\partial u_z}{\partial z}\right)\right] = 0 \quad , \quad (4)$$

where p is the pressure, and μ is the dynamic viscosity.

The energy conservation equation is given by

$$\frac{\partial(\rho u_x h)}{\partial x} + \frac{\partial(\rho u_y h)}{\partial y} + \frac{\partial(\rho u_z h)}{\partial z} + \frac{\partial}{\partial x}\left(\rho \sum_{k=1}^{\gamma} w_k h_k V_{k,x} - k_g \frac{\partial T}{\partial x}\right)$$
$$+\frac{\partial}{\partial y}\left(\rho \sum_{k=1}^{\gamma} w_k h_k V_{k,y} - k_g \frac{\partial T}{\partial y}\right) + \frac{\partial}{\partial z}\left(\rho \sum_{k=1}^{\gamma} w_k h_k V_{k,z} - k_g \frac{\partial T}{\partial z}\right) = 0 \quad , \quad (5)$$

where h is the enthalpy, k is the thermal conductivity, T is the temperature, γ is the total number of gaseous species, w is the mass fraction, and V is the diffusion velocity. The subscripts k and g denote gaseous species k and the gas mixture, respectively.

The species conservation equation can be written as

$$\frac{\partial(\rho u_x w_k)}{\partial x} + \frac{\partial(\rho u_y w_k)}{\partial y} + \frac{\partial(\rho u_z w_k)}{\partial z} + \frac{\partial}{\partial x}\left(\rho w_k V_{k,x}\right)$$
$$+\frac{\partial}{\partial y}\left(\rho w_k V_{k,y}\right) + \frac{\partial}{\partial z}\left(\rho w_k V_{k,z}\right) - \dot{\xi}_k W_k = 0, \ k = 1,\dots,K_g \quad , \quad (6)$$

where W is the molecular mass, and $\dot{\xi}$ is the rate of production by gas-phase reaction.

The surface species conservation equation is given by

$$\theta_m \dot{\zeta}_m \Gamma^{-1} = 0, \ \omega = \gamma+1,\dots,\gamma+\delta \ , \quad (7)$$

where θ is the coverage, ω and δ are the total number of chemical species and surface species, respectively, Γ is the active site density, and $\dot{\zeta}$ is the rate of production by surface reaction. The subscript m denotes surface species m.

The energy conservation equation of the solid phase can be written as

$$\frac{\partial}{\partial x}\left(k_s \frac{\partial T}{\partial x}\right) + \frac{\partial}{\partial y}\left(k_s \frac{\partial T}{\partial y}\right) + \frac{\partial}{\partial z}\left(k_s \frac{\partial T}{\partial z}\right) = 0. \quad (8)$$

where the subscript s denotes the solid walls.

The surface species conservation equations are given by

$$\eta \alpha W_k (\dot{s}_k)_\psi + (\rho w_k V_{k,y})_\psi = 0, \ k = 1,\dots,K_g , \quad (9)$$
$$\eta \alpha W_k (\dot{s}_k)_\psi + (\rho w_k V_{k,z})_\psi = 0, \ k = 1,\dots,K_g . \quad (10)$$

in which α is the surface area factor.

The effective diffusivity is defined as

$$\frac{1}{D_i'} = \frac{1}{\varepsilon_p}\tau_p\left(\frac{1}{D_i^m} + \frac{1}{D_i^K}\right). \quad (11)$$

where ε_p is the porosity, τ_p is the tortuosity factor, and D^m and D^k are the molecular diffusivity and Knudsen diffusivity, respectively.

The Knudsen diffusivity is defined as

$$D_i^K = \frac{d}{3}(8RT)^{\frac{1}{2}}(\pi W_i)^{-\frac{1}{2}}. \quad (12)$$

wherein d is the mean pore diameter.

The effective thermal conductivity k' is defined as

$$k' = \varepsilon_p k_g + (1-\varepsilon_p)k . \quad (13)$$

At the solid-gas phase boundaries, the energy conservation equation is given by

$$k_s\left(\frac{\partial T}{\partial y}\right)_{\psi+} + k_s\left(\frac{\partial T}{\partial z}\right)_{\psi+} + \sum_{k=1}^{K_g}(\dot{s}_k h_k W_k)_\psi$$
$$-k_g\left(\frac{\partial T}{\partial y}\right)_{\psi-} - k_g\left(\frac{\partial T}{\partial z}\right)_{\psi-} = 0 \quad . \quad (14)$$

The typical mesh consists of about 600,000 nodes in total. The second-order upwind scheme is used for the convection terms of each governing equation. The under-relaxation parameters are reduced for all variables. Convergence is judged by examining residual levels.

2.3. Chemical kinetic models

The combustion catalyst comprises a mixture of copper-oxide and zinc-oxide that are supported on an alumina carrier [53]. Additionally, the reforming catalyst comprises a mixture of copper and zinc-oxide that are supported on an alumina carrier [54]. Unfortunately, balancing the heat requirements of the endothermic reaction with the heat generated by the exothermic reaction is extraordinarily difficult [55]. For example, maintaining the temperature of methanol steam reforming at or below 300 °C is very difficult when heat is supplied by catalytic combustion, which typically runs above 500 °C. In particular, the combustion reaction is difficult to control with convenient combustion catalysts and fuels [56], and most of the combustion occurs near the fuel inlet. This uneven combustion results in uneven heat transfer to the endothermic reaction and poor overall reactor performance [57, 58]. In such a context, a copper-oxide-based catalyst with relatively low catalytic activity is used for the combustion of methanol, as described above.
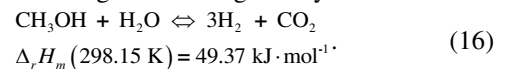
The exothermic, catalytic combustion reaction is given by

$$CH_3OH + 1.5O_2 \Leftrightarrow 2H_2O + CO_2$$
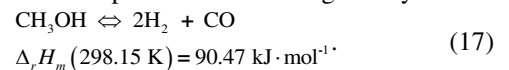$$\Delta_r H_m(298.15 \text{ K}) = -726.60 \text{ kJ}\cdot\text{mol}^{-1} , \quad (15)$$
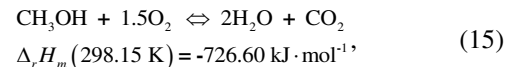
wherein $\Delta_r H_m$ is the standard molar enthalpy of reaction. Homogeneous combustion is not accounted for, as the desired operating temperatures are low for the reactor.
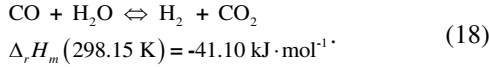
The steam reforming reaction is given by

$$CH_3OH + H_2O \Leftrightarrow 3H_2 + CO_2$$
$$\Delta_r H_m(298.15 \text{ K}) = 49.37 \text{ kJ}\cdot\text{mol}^{-1} . \quad (16)$$

The methanol decomposition reaction is given by

$$CH_3OH \Leftrightarrow 2H_2 + CO$$
$$\Delta_r H_m(298.15 \text{ K}) = 90.47 \text{ kJ}\cdot\text{mol}^{-1} . \quad (17)$$

The water-gas shift reaction is described by

$$CO + H_2O \Leftrightarrow H_2 + CO_2$$
$$\Delta_r H_m (298.15\ K) = -41.10\ kJ \cdot mol^{-1}. \quad (18)$$

The combustion process is modeled by the kinetic model [53], and the reforming process is modeled by the kinetic model [54]. For the reforming reaction, the rate equation can be written as

$$r_{reforming} = \begin{bmatrix} k_R K^*_{CH_3O^{(1)}} \left(p_{CH_3OH} p_{H_2}^{-0.5} \right) \\ \cdot \left(1 - k_R^{-1} p_{H_2}^3 p_{CO_2} p_{CH_3OH}^{-1} p_{H_2O}^{-1} \right) c_{S_1}^T c_{S_{1a}}^T \end{bmatrix}$$
$$\cdot \begin{pmatrix} 1 + K^*_{CH_3O^{(1)}} \left(p_{CH_3OH} p_{H_2}^{-0.5} \right) \\ + K^*_{HCOO^{(1)}} p_{CO_2} p_{H_2}^{0.5} + K^*_{OH^{(1)}} \left(p_{H_2O} p_{H_2}^{-0.5} \right) \end{pmatrix}^{-1}, \quad (19)$$
$$\cdot \left(1 + K^{0.5}_{H^{(1a)}} p_{H_2}^{0.5} \right)^{-1}$$

where r is the reaction rate, $c_{S_i}^T$ is the total surface concentration of site i, K is the equilibrium constant, k is the rate constant, the superscript (i) denotes the species adsorbed on active site i, the superscript $*$ denotes the composite parameter, and the subscripts 1 and $1a$ denote the species index.

For the water-gas shift reaction, the rate equation can be written as

$$r_{water-gas\ shift} = \begin{bmatrix} k_W^* K^*_{OH^{(1)}} \left(p_{CO} p_{H_2O} p_{H_2}^{-0.5} \right) \\ \cdot \left(1 - k_W^{-1} p_{H_2} p_{CO_2} p_{CO}^{-1} p_{H_2O}^{-1} \right) c_{S_1}^{T^2} \end{bmatrix}$$
$$\cdot \left[\begin{pmatrix} 1 + K^*_{CH_3O^{(1)}} \left(p_{CH_3OH} p_{H_2}^{-0.5} \right) \\ + K^*_{HCOO^{(1)}} p_{CO_2} p_{H_2}^{0.5} + K^*_{OH^{(1)}} \left(p_{H_2O} p_{H_2}^{-0.5} \right) \end{pmatrix} \right]^{-2}, \quad (20)$$

For the decomposition reaction, the rate equation can be written as

$$r_{decomposition} = \begin{bmatrix} k_D K^*_{CH_3O^{(2)}} \left(p_{CH_3OH} p_{H_2}^{-0.5} \right) \\ \cdot \left(1 - k_D^{-1} p_{H_2}^2 p_{CO} p_{CH_3OH}^{-1} \right) c_{S_2}^T c_{S_{2a}}^T \end{bmatrix}$$
$$\cdot \left[\begin{pmatrix} 1 + K^*_{CH_3O^{(2)}} \left(p_{CH_3OH} p_{H_2}^{-0.5} \right) \\ + K^*_{OH^{(2)}} \left(p_{H_2O} p_{H_2}^{-0.5} \right) \end{pmatrix} \left(1 + K^{0.5}_{H^{(2a)}} p_{H_2}^{0.5} \right) \right]^{-1}, \quad (21)$$

where the subscripts 2 and $2a$ denote the species index.

2.4. Validation of the model

To verify the model's accuracy, the predictions are compared with the data obtained from experimental measurements [59, 60]. The cross-sectional shape of the channels is rectangular. The channels have a height of 0.6 mm, a width of 0.5 mm, and a length of 33.0 mm. The steam-to-carbon molar ratio is 1.1, and the reaction temperature varies from 473 to 533 K. Computational fluid dynamics simulations are performed for the reactor with rectangular channels under the conditions described in detail above, and the numerical results are compared with the experimental data. The methanol conversion and hydrogen production rate are plotted in Fig. 2 against temperature. The predictions are in satisfactory agreement with the data obtained from experimental measurements.
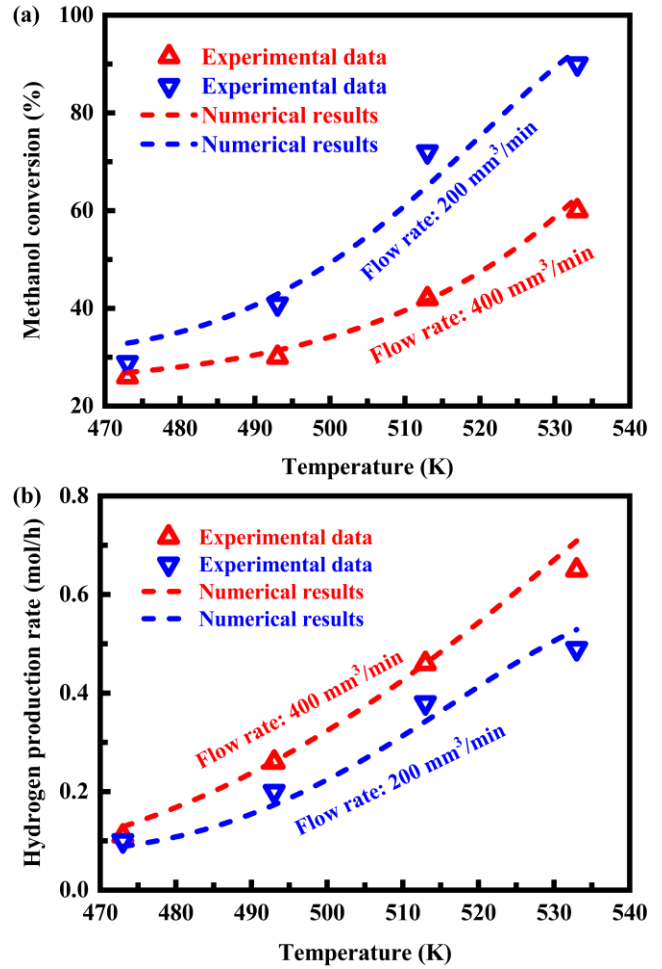

Fig. 2. (a) Methanol conversion and (b) hydrogen production rate at different reaction temperatures. The experimental data [59, 60] are included for comparison.

3. Results and Discussion

3.1. Overall heat transfer characteristics

The contour plots of temperature and specific enthalpy are illustrated in Fig. 3 for the reactor. The thermal energy released from the combustion channels is conducted through the channel walls to reforming channels, thereby supporting the endothermic conversion reaction. Efficient transfer of thermal energy is achieved within the reactor, as illustrated in Fig. 3. To enhance heat transfer within the reactor by dramatically increasing heat transfer area, the flow channels could contain internal, function fins [61], for example, castellated walls, or any other type of walls [62], such as grooved, serpentine or any other design. The geometry and dimensions of the flow channels may vary depending upon the design parameters of the reaction system [63, 64]. However, the flow channels must be designed to allow intimate thermal contact whilst keeping the streams from becoming mixed.
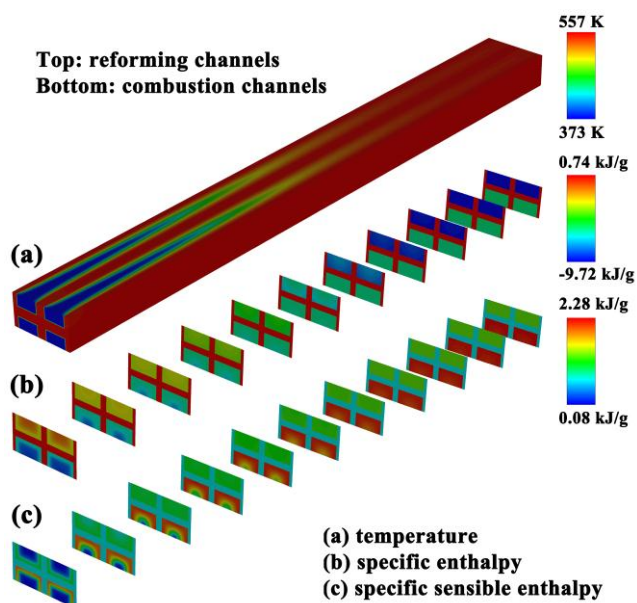
Fig. 3. Contour plots of temperature and specific enthalpy for the reactor. The channels are square in cross section.
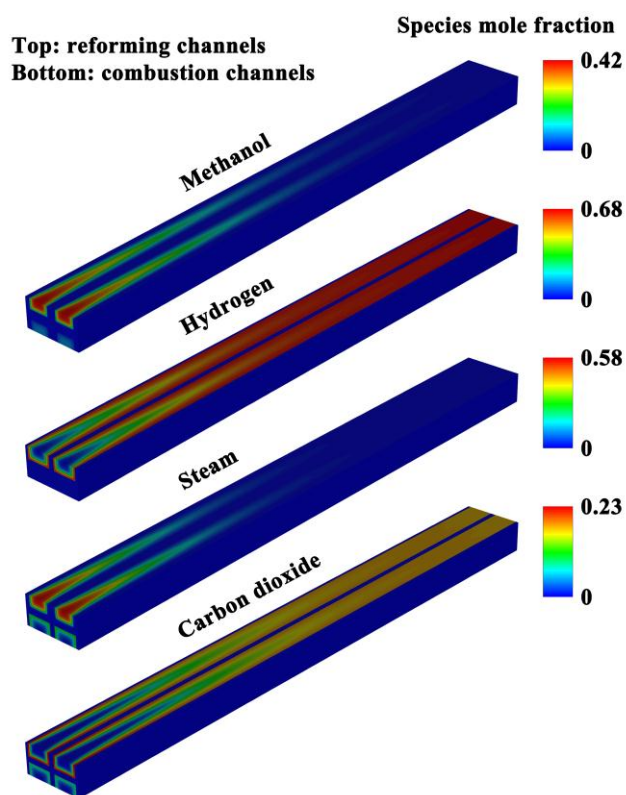

Fig. 4. Contour plots of species mole fractions for the reactor. The species mole fractions are plotted on contour maps to provide a visual presentation of composition changes.

The temperature rises very quickly in the reactor, as illustrated in Fig. 3, reaching about 560 K. High temperatures would potentially destroy or deactivate the catalyst layers of the reactor and may pose a risk to the structural integrity of the reactor. Within the channel walls, a substantially uniform temperature profile is achieved, as illustrated in Fig. 3, because of the excellent heat conduction properties of the channel walls, which can improve the performance of the reaction system with increased conversion due to their high thermal conductivity. The contour plots of species mole fractions are illustrated in Fig. 4 for the reactor. Nearly complete conversion to hydrogen is achieved and the rate of conversion is high due to the excellent heat conduction properties of the channel walls.

Instead of temperature, a change in enthalpy or sensible enthalpy can be used as the state variable to account for simplifying the description of heat transfer. For the mixtures, the enthalpy correlates to their thermal energy. The change in enthalpy for the reforming process is the heat absorbed by the endothermic reactant stream. The change in enthalpy for the combustion process is the heat released by the exothermic reactant stream. There is a significant change in specific enthalpy or specific sensible enthalpy along the streamwise direction, as illustrated in Fig. 3, especially near the channel inlets. Accordingly, the conversion occurs very rapidly near the channel inlets and almost complete conversion is achieved, as illustrated in Fig. 4. This is because excellent wall heat conduction properties tend to facilitate the conversion.

For the exothermic catalytic combustion reaction, the change in total enthalpy is negative, since the total enthalpy of combustion products is smaller than that of the reactants of the reaction. The change in total enthalpy is equal to the heat released by the exothermic reaction. For the reforming reaction, the change in total enthalpy is positive, since the total enthalpy of reforming products is larger than that of the reactants of the reaction. The change in total enthalpy is equal to the heat absorbed by the endothermic reaction. However, these results can be applied only to total enthalpy. When applied to specific enthalpy, the change in specific enthalpy is positive for the exothermic catalytic combustion reaction and the change in specific enthalpy is negative for the endothermic reaction, as illustrated in Fig. 3. However, the change in specific sensible enthalpy is always positive, especially for the exothermic process. This is because the temperature of the streams will continue to rise along the streamwise direction. On the other hand, the concentration of species has a steep gradient in the flow channels, as illustrated in Fig. 4, especially near the channel inlets. This is caused by the small dimensions of the parallel channels and the high rates of the reactions. From an economic standpoint, it is desirable to minimize capital cost while preserving conversion yields through process intensification.

3.2. Effect of wall heat conduction properties

The effect of wall heat conduction properties on the temperature field within the reactor is investigated. The results are presented in Fig. 5, in which the two-dimensional contour plots of temperature are illustrated for

the reactor. The thermal conductivity of the channel walls varies from 0.2 to 200 W/(m·K). The temperature increases with decreasing the wall thermal conductivity. For the reactor, the desired reaction temperatures can influence the choice of channel wall material. For example, when chosen for the channel walls, the material should not impede on the transport of thermal energy between the endothermic and exothermic streams within the reactor, in addition to a suitable melting point. Within the channel walls, a substantially uniform temperature profile is achieved in the case of a high thermal conductivity of 200 W/(m·K). For example, the excellent heat conduction properties enable a more uniform distribution of temperature along the streamwise direction. This causes a reduction of peak temperature within the reactor, thereby ensuring the structural integrity of the reaction system and prolonging the life of the catalytically active materials. Therefore, the channel walls of the reactor must be formed using materials with excellent heat conduction properties. In this context, thermally conductive ceramics and metals are well-suited.
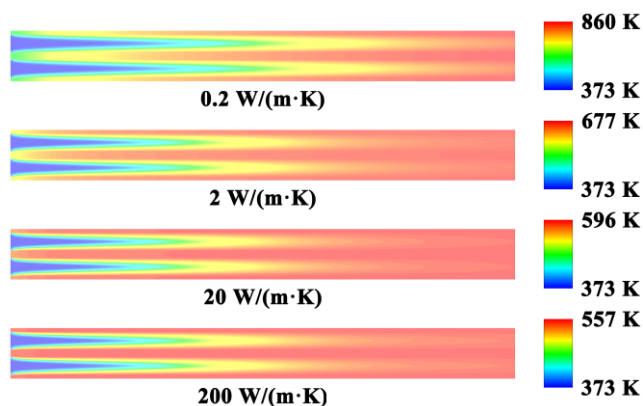

Fig. 5. Two-dimensional contour plots of temperature for the reactor. The thermal conductivity of the channel walls varies from 0.2 to 200 W/(m·K).

The effect of wall heat conduction properties on methanol conversion is investigated. The results are presented in Fig. 6, in which methanol conversion is plotted against the thermal conductivity of the channel walls. The wall thermal conductivity varies from 0.2 to 200 W/(m·K). As the wall thermal conductivity increases, methanol conversion increases. Wall materials with poor heat conduction properties degrade the reactor performance. Therefore, materials with excellent heat conduction properties are preferred for the reaction system, as discussed above. The channel wall material should be selected with a thermal conductivity at least higher than 20 W/(m·K). For example, copper can be employed as the channel wall material because of it very high thermal conductivity. Even at room temperature, the thermal conductivity of copper can be as high as about 400 W/(m·K), thereby preventing the formation of hot spots. Additionally, this metal material is cost effective.
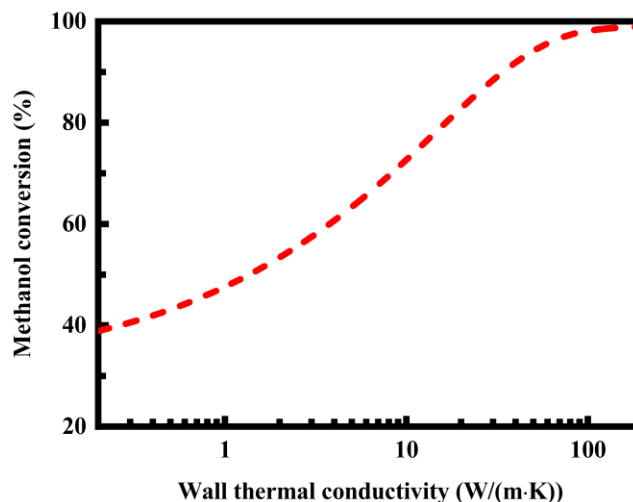

Fig. 6. Effect of wall heat conduction properties on methanol conversion. The thermal conductivity of the channel walls varies from 0.2 to 200 W/(m·K).

3.3. Reaction heat fluxes

The reaction heat fluxes are investigated to better understand the thermal coupling between the endothermic and exothermic streams. The results are presented in Fig. 7, in which the endothermic and exothermic reaction heat fluxes are plotted against the streamwise distance. The channels are 0.7 mm in width. Heat flux is a vector quantity, and therefore the heat flux is negative for the endothermic steam reforming reaction. The exothermic heat flux is greater than the absolute value of the endothermic heat flux. The peak exothermic heat flux is located upstream of the peak endothermic heat flux. An un-uniform catalyst distribution could be employed for the rector so as to provide optimum synchronization of the reaction fluxes of heat consumption and generation in the endothermic reforming and exothermic combustion channels, respectively.
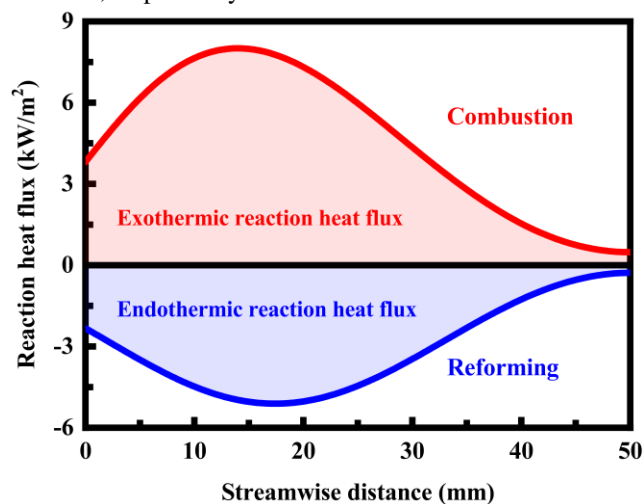

Fig. 7. Endothermic and exothermic reaction heat fluxes as a function of the streamwise distance. The channels are 0.7 mm in width.

The effect of channel dimensions on endothermic and exothermic reaction heat fluxes is illustrated in Fig. 8. Modifications and variations are made by increasing the dimensions of the channels. The channel dimensions are important factors in practical applications [65, 66]. The channels are 0.7 and 2.0 mm, respectively, in width, but the flow rate remains constant for each process. The evolution of the reaction heat fluxes is illustrated for the two cases. The location of the reaction heat flux peak shifts in channel dimensions. More specifically, as the channel dimensions increase while maintaining the flow rates, the peak of the reaction heat fluxes shifts upstream, causing an increase in the peak reaction heat flux. Intuitively, as the channel dimensions decrease while maintaining the flow rates, the peak of the reaction heat fluxes will shift downstream.
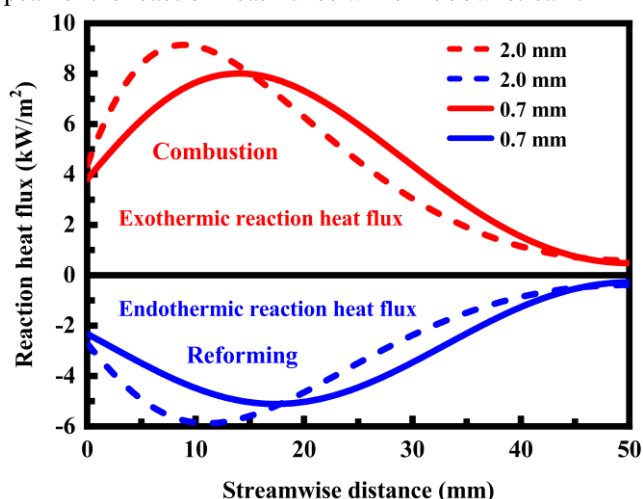

Fig. 8. Effect of channel dimensions on endothermic and exothermic reaction heat fluxes. The channels are 0.7 and 2.0 mm, respectively, in width.

4. Conclusions

Numerical simulations are conducted to better understand the consumption, generation, and exchange of thermal energy in a microchannel reforming reactor. The effects of wall heat conduction properties and channel dimensions on heat transfer characteristics and reactor performance are investigated. The results indicate that the thermal conductivity of the channel walls is fundamentally important. The change in specific enthalpy is positive for the exothermic reaction and negative for the endothermic reaction. The change in specific sensible enthalpy is always positive, especially for the exothermic process. Materials with high thermal conductivity are preferred for the channel walls, thereby improving the thermal effectiveness of the system. Thermally conductive ceramics and metals are well-suited, which can promote overall heat transfer and levels of conversion. Wall materials with poor heat conduction properties degrade the reactor performance, since the design will lead to reduced heat transfer and therefore chemical conversion. Materials with low thermal conductivity suffer from heat transfer limitation and pose a risk to the structural integrity of the reactor and reduce the life of the catalysts. Reaction heat flux profiles are considerably affected by channel dimensions. The peak reaction heat flux increases with the channel dimensions while maintaining the flow rates.

Conflict of Interest

The authors declare that they have no conflict of interest

References

[1] Amiri, T. Y., Ghasemzageh, K., Iulianelli, A. (2020) Membrane reactors for sustainable hydrogen production through steam reforming of hydrocarbons: A review. Chemical Engineering and Processing - Process Intensification, 157, 108148.

[2] Sá, S., Silva, H., Brandão, L., Sousa, J. M., Mendes, A. (2010) Catalysts for methanol steam reforming-A review. Applied Catalysis B: Environmental, 99(1-2), 43-57.

[3] Dincer, I. (2012) Green methods for hydrogen production. International Journal of Hydrogen Energy, 37(2), 1954-1971.

[4] Muradov N. Z., Veziroğlu, T. N. (2005) From hydrocarbon to hydrogen-carbon to hydrogen economy. International Journal of Hydrogen Energy, 30(3), 225-237.

[5] Tacchino, V., Costamagna, P., Rosellini, S., Mantelli, V., Servida, A. (2022) Multi-scale model of a top-fired steam methane reforming reactor and validation with industrial experimental data. Chemical Engineering Journal, 428, 131492.

[6] Tutar, M., Üstün, C. E., Campillo-Robles, J. M., Fuente, R., Cibrián, S., Arzua, I., Fernández, A., López, G.A. (2021) Optimized CFD modelling and validation of radiation section of an industrial top-fired steam methane reforming furnace. Computers & Chemical Engineering, 155, 107504.

[7] Wang, J., Wei, S., Wang, Q., Sundén, B. (2021) Transient numerical modeling and model predictive control of an industrial-scale steam methane reforming reactor. International Journal of Hydrogen Energy, 46(29), 15241-15256.

[8] Taji, M., Farsi, M., Keshavarz, P. (2018) Real time optimization of steam reforming of methane in an industrial hydrogen plant. International Journal of Hydrogen Energy, 43(29), 13110-13121.

[9] Fadzillah, D. M., Kamarudin, S. K., Zainoodin, M. A., Masdar, M. S. (2019) Critical challenges in the system development of direct alcohol fuel cells as portable power supplies: An overview. International Journal of Hydrogen Energy, 44(5), 3031-3054.

[10] Wang, Y., Diaz, D. F. R., Chen, K. S., Wang, Z., Adroher, X. C. (2020) Materials, technological status, and fundamentals of PEM fuel cells - A review. Materials Today, 32, 178-203.

[11] Zhang, X., Jin, Y., Li, D., Xiong, Y. (2021) A review on recent advances in micro-tubular solid oxide fuel cells. Journal of Power Sources, 506, 230135.

[12] Alias, M. S., Kamarudin, S. K., Zainoodin, A. M., Masdar, M. S. (2020) Active direct methanol fuel cell: An overview. International Journal of Hydrogen Energy, 45(38), 19620-19641.

[13] Luo, M, Zhang, J., Zhang, C., Chin, C. S., Ran, H., Fan, M., Du, K., Shuai, Q. (2022) Cold start investigation of fuel cell vehicles with coolant preheating strategy. Applied Thermal Engineering, 201, 117816.

[14] Wei, X., Leng, J., Sun, C., Huo, W., Ren, Q., Sun, F. (2022) Co-optimization method of speed planning and energy management for fuel cell vehicles through signalized intersections. Journal of Power Sources, 518, 230598.

[15] Rakib, M. A., Grace, J. R., Lim, C. J., Elnashaie, S. S. E. H. (2010) Steam reforming of heptane in a fluidized bed membrane reactor. Journal of Power Sources, 195(17), 5749-5760.

[16] Abashar, M. E. E. (2013) Steam reforming of n-heptane for production of hydrogen and syngas. International Journal of Hydrogen Energy, 38(2), 861-869.

[17] Park, S., Yoo, J., Han, S. J., Song, J. H., Lee, E. J., Song, I. K. (2017) Steam reforming of liquefied natural gas (LNG) for hydrogen production over nickel-boron-alumina xerogel catalyst. International Journal of Hydrogen Energy, 42(22), 15096-15106.

[18] Bang, Y., Han, S. J., Seo, J. G., Youn, M. H., Song, J. H., Song, I. K. (2012) Hydrogen production by steam reforming of liquefied natural gas (LNG) over ordered mesoporous nickel-alumina catalyst. International Journal of Hydrogen Energy, 37(23), 17967-17977.

[19] Wang, Y., Sun, K., Zhang, S., Xu, L., Hu, G., Hu, X. (2021) Steam reforming of alcohols and carboxylic acids: Importance of carboxyl and alcoholic hydroxyl groups on coke properties. Journal of the Energy Institute, 98, 85-97.

[20] Li, Y., Zhang, L., Zhang, Z., Liu, Q., Zhang, S., Liu, Q., Hu, G., Wang, Y., Hu, X. (2019) Steam reforming of the alcohols with varied structures: Impacts of acidic sites of Ni catalysts on coking. Applied Catalysis A: General, 584, 117162.

[21] Guo, Y., Li, H., Kameyama, H. (2011) Steam reforming of kerosene over a metal-monolithic alumina-supported Ru catalyst: Effect of preparation conditions and electrical-heating test. Chemical Engineering Science, 66(23), 6287-6296.

[22] Chick, L. A., Marina, O. A., Coyle, C. A., Thomsen, E. C. (2013) Effects of temperature and pressure on the performance of a solid oxide fuel cell running on steam reformate of kerosene. Journal of Power Sources, 236, 341-349.

[23] Koga, M., Watanabe, T. (1991) Plate type reformer. United States Patent Number: 5015444, Assignee: Ishikawajima-Harima Heavy Industries Co., Ltd., Tokyo, Application Number: 7.243334.

[24] Igarashi, A., Fukuhara, C., Takeshita, S., Nishino, C., Hanawa, M. (1992) Apparatus and method for preparing reformed gas by means of electroless plating. United States Patent Number: 5167865, Assignee: Mitsubishi Petrochemical Engineering Company Limited, Tokyo, Application Number: 7.574099.

[25] Fukuhara, C., Igarashi, A. (2005) Performance simulation of a wall-type reactor in which exothermic and endothermic reactions proceed simultaneously, comparing with that of a fixed-bed reactor. Chemical Engineering Science, 60(24), 6824-6834.

[26] Kawamura, Y., Ogura, N., Yamamoto, T., Igarashi, A. (2006) A miniaturized methanol reformer with Si-based microreactor for a small PEMFC. Chemical Engineering Science, 61(4), 1092-1101.

[27] Ioannides, T., Verykios, X. E. (1998) Development of a novel heat-integrated wall reactor for the partial oxidation of methane to synthesis gas. Catalysis Today, 46(2-3), 71-81.

[28] Piga, A., Verykios, X. E. (2000) An advanced reactor configuration for the partial oxidation of methane to synthesis gas. Catalysis Today, 60(1-2), 63-71.

[29] Loffler, D. A., Faz, C. E., Sokolovskii, V., Iglesia, E. (2002) Catalytic separator plate reactor and method of catalytic reforming of fuel to hydrogen. United States Patent Publication Number: 20020168308, Application Number: 09972142.

[30] Loffler, D. (2005) Systems and methods for generating hydrogen from hycrocarbon fuels. United States Patent Publication Number: 20050229491, Applicant: Nu Element, Inc., Tacoma, Washington, Application Number: 11.050371.

[31] Tonkovich, A. L., Roberts, G., Perry, S. T., Fitzgerald, S. P., Wegeng, R. S., Wang, Y., Vanderwiel, D., Marco, J. L. (2016) Integrated reactors, methods of making same, and methods of conducting simultaneous exothermic and endothermic reactions. United States Patent Number: 9452402, Assignee: Battelle Memorial Institute, Richland, Washington, Application Number: 14.053500.

[32] Tonkovich, A. L., Roberts, G. L., Perry, S. T., Fitzgerald, S. P. (2005) Methods of conducting simultaneous exothermic and endothermic reactions. United States Patent Number: 6969506, Assignee: Battelle Memorial Institute, Richland, Washington, Application Number: 10.076875.

[33] Brown, R. C. (2020) Process intensification through directly coupled autothermal operation of chemical reactors. Joule, 4(11), 2268-2289.

[34] Tonkovich, A. Y., Perry, S., Wang, Y., Qiu, D., LaPlante, T., Rogers, W. A. (2004) Microchannel process technology for compact methane steam reforming. Chemical Engineering Science, 59(22-23), 4819-4824.

[35] Roychowdhury, S., Sundararajan, T., Das, S. K. (2019) Conjugate heat transfer studies on steam reforming of ethanol in micro-channel systems. International Journal of Heat and Mass Transfer, 139, 660-674.

[36] Tonkovich, A. L. Y., Yang, B., Perry, S. T., Fitzgerald, S. P., Wang, Y. (2007) From seconds to milliseconds to microseconds through tailored microchannel reactor design of a steam methane reformer. Catalysis Today, 120(1), 21-29.

[37] Mettler, M. S., Stefanidis, G. D., Vlachos, D. G. (2011) Enhancing stability in parallel plate microreactor stacks for syngas production. Chemical Engineering Science, 66(6), 1051-1059.

[38] Cao, C., Zhang, N., Dang, D., Cheng, Y. (2017) Numerical evaluation of a microchannel methane reformer used for miniaturized GTL: Operating characteristics and greenhouse gases emission. Fuel Processing Technology, 167, 78-91.

[39] Tonkovich, A., Kuhlmann, D., Rogers, A., McDaniel, J., Fitzgerald, S., Arora, R., Yuschak, T. (2005) Microchannel technology scale-up to commercial capacity. Chemical Engineering Research and Design, 83(6), 634-639.

[40] Gavriilidis, A., Angeli, P., Cao, E., Yeong, K. K., Wan, Y. S. S. (2002) Technology and applications of microengineered reactors. Chemical Engineering Research and Design, 80(1), 3-30.

[41] Lerou, J. J., Tonkovich, A. L., Silva, L., Perry, S., McDaniel, J. (2010) Microchannel reactor architecture enables greener processes. Chemical Engineering Science, 65(1), 380-385.

[42] Murphy, D. M., Manerbino, A., Parker, M., Blasi, J., Kee, R. J., Sullivan, N. P. (2013) Methane steam reforming in a novel ceramic microchannel reactor. International Journal of Hydrogen Energy, 38(21), 8741-8750.

[43] Baldea, M., Daoutidis, P. (2007) Dynamics and control of autothermal reactors for the production of hydrogen. Chemical Engineering Science, 62(12), 3218-3230.

[44] Zanfir, M., Gavriilidis, A. (2004) Influence of flow arrangement in catalytic plate reactors for methane steam reforming. Chemical Engineering Research and Design, 82(2), 252-258.

[45] Kolios, G., Frauhammer, J., Eigenberger, G. (2000) Autothermal fixed-bed reactor concepts. Chemical Engineering Science, 55(24), 5945-5967.

[46] Tiemersma, T. P., Kolkman, T., Kuipers, J. A. M., Annaland, M. V. S. (2012) A novel autothermal reactor concept for thermal coupling of the exothermic oxidative coupling and endothermic steam reforming of methane. Chemical Engineering Journal, 203, 223-230.

[47] Herdem, M. S., Mundhwa, M., Farhad, S., Hamdullahpur, F. (2019) Catalyst layer design and arrangement to improve the performance of a microchannel methanol steam reformer. Energy Conversion and Management, 180, 149-161.

[48] Engelbrecht, N., Everson, R. C., Bessarabov, D., Kolb, G. (2020) Microchannel reactor heat-exchangers: A review of design strategies for the effective thermal coupling of gas phase reactions. Chemical Engineering and Processing - Process Intensification, 157, 108164.

[49] Palo, D. R., Dagle, R. A., Holladay, J. D. (2007) Methanol steam reforming for hydrogen production. Chemical Reviews, 107(10), 3992-4021.

[50] Patel, S., Pant, K. K. (2006) Activity and stability enhancement of copper-alumina catalysts using cerium and zinc promoters for the selective production of hydrogen via steam reforming of methanol. Journal of Power Sources, 159(1), 139-143.

[51] Stefanidis, G. D., Vlachos, D. G. (2009) High vs. low temperature reforming for hydrogen production via microtechnology. Chemical Engineering Science, 64(23), 4856-4865.

[52] Tonkovich, A. Y., Perry, S., Wang, Y., Qiu, D., LaPlante, T., Rogers, W. A. (2004) Microchannel process technology for compact methane steam reforming. Chemical Engineering Science, 59(22-23), 4819-4824.

[53] Reitz, T. L., Ahmed, S., Krumpelt, M., Kumar, R., Kung, H. H. (2000) Characterization of CuO/ZnO under oxidizing conditions for the oxidative methanol reforming reaction. Journal of Molecular Catalysis A: Chemical, 162(1-2), 275-285.

[54] Peppley, B. A., Amphlett, J. C., Kearns, L. M., Mann, R. F. (1999) Methanol-steam reforming on Cu/ZnO/Al$_2$O$_3$ catalysts. Part 2. A comprehensive kinetic model. Applied Catalysis A: General, 179(1-2), 31-49.

[55] Zanfir, M., Gavriilidis, A. (2003) Catalytic combustion assisted methane steam reforming in a catalytic plate reactor. Chemical Engineering Science, 58(17), 3947-3960.

[56] Pasel, J., Emonts, B., Peters, R., Stolten, D. (2001) A structured test reactor for the evaporation of methanol on the basis of a catalytic combustion. Catalysis Today, 69(1-4), 193-200.

[57] Zhai, X., Ding, S., Cheng, Y., Jin, Y., Cheng, Y. (2010) CFD simulation with detailed chemistry of steam reforming of methane for hydrogen production in an integrated micro-reactor. International Journal of Hydrogen Energy, 35(11), 5383-5392.

[58] Cao, C., Zhang, N., Chen, X., Cheng, Y. (2015) A comparative study of Rh and Ni coated microchannel reactor for steam methane reforming using CFD with detailed chemistry. Chemical Engineering Science, 137, 276-286.

[59] Park, G. G., Seo, D. J., Park, S. H., Yoon, Y. G., Kim, C. S., Yoon, W. L. (2004) Development of microchannel methanol steam reformer. Chemical Engineering Journal, 101(1-3), 87-92.

[60] Park, G. G., Yim, S. D., Yoon, Y. G., Kim, C. S., Seo, D. J., Eguchi, K. (2005) Hydrogen production with integrated microchannel fuel processor using methanol for portable fuel cell systems. Catalysis Today, 110(1-2), 108-113.

[61] Chu, X., Zeng, X., Zheng, T., Zhuang, W., Yang, Y., Zhou, W., Hong, Y. (2020) Structural design and performance research of methanol steam reforming microchannel for hydrogen production based on mixing effect. International Journal of Hydrogen Energy, 45(41), 20859-20874.

[62] Lu, W., Zhang, R., Toan, S., Xu, R., Zhou, F., Sun, Z., Sun, Z. (2022) Microchannel structure design for hydrogen supply from methanol steam reforming. Chemical Engineering Journal, 429, 132286.

[63] Stefanidis, G. D., Vlachos, D. G., Kaisare, N. S., Maestri, M. (2009) Methane steam reforming at microscales: Operation strategies for variable power output at millisecond contact times. AIChE Journal, 55(1), 180-191.

[64] Stefanidis, G. D., Vlachos, D. G. (2008) Millisecond methane steam reforming via process and catalyst intensification. Chemical Engineering & Technology, 31(8), 1201-1209.

[65] Zanfir, M., Gavriilidis, A. (2002) An investigation of catalytic plate reactors by means of parametric sensitivity analysis. Chemical Engineering Science, 57(9), 1653-1659.

[66] Cao, C., Dang, D., Li, Y., Xu, J., Cheng, Y. (2018) Managing temperature uniformity of thermally integrated micro reformers with different axial dimensions: A detailed numerical study. Chemical Engineering and Processing - Process Intensification, 132, 218-228.

Recommended Citation